

Characterization of Aseismic Fault-Slip in a Deep Hard Rock Mine Through Numerical Modelling: Case Study

Atsushi Sainoki¹ · Hani S. Mitri² · Damodara Chinnasane³

Received: 11 November 2016 / Accepted: 20 June 2017 / Published online: 1 July 2017
© Springer-Verlag GmbH Austria 2017

Abstract Seismic moment is a predominantly utilized parameter for assessing fault-slip potential when the numerical modelling of fault-slip is carried out. However, relying on seismic moment as an indicator for fault-slip might lead to incorrect conclusions, as fault-slip can be inherently seismic or aseismic. The present study examines the behaviour of a fault in Copper Cliff Mine, Canada, with a 3D numerical model encompassing major geological structures in the area of interest. Three types of numerical analyses are conducted, namely elastic and elasto-plastic analyses in static conditions and elasto-plastic analysis in dynamic conditions. The static analyses show that the fault most likely had undergone shear failure at the pre-mining stage. It is then demonstrated that mining activities induce further shear movements along the fault plane as well as within the fault material, as the fault is composed of thick, severely fractured materials. Notwithstanding the results, no large seismic events with $M_w > 0.1$ were recorded within the fault from microseismic-monitoring systems between 2006 and 2014, implying that the shear movements are aseismic and static. Furthermore, microseismic database analysis using 350,000 events that took place between 2004 and 2014 indicates that the fault is not seismically active. It is found from the dynamic analysis that the maximum slip rate during fault-slip is not more than 0.3 m/s, even when the fault-slip is simulated with an

instantaneous stress drop. This result substantiates the assumption that the fault is not seismically active and shear movements are dominantly aseismic. It is therefore suggested that other factors such as stress re-distribution induced by the aseismic slip be considered in order to assess damage that could be caused by the fault movements. The present study sheds light on the importance of distinguishing aseismic from seismic fault-slip for optimizing support systems in underground mines.

Keywords Aseismic fault-slip · Fault-slip potential · Dynamic analysis, underground mine · Numerical analysis

1 Introduction

The shear slip behaviour of faults in response to stress re-distribution due to mining activities can be classified as either seismic, i.e. exhibiting high slip rate, or aseismic. The former is generally described as mining-induced fault-slip resulting in instantaneous shear movement of a pre-existing fault or sudden shear rupture through intact rock that is induced by stress re-distribution due to mining activities. The latter is characterized by quasi-static shear movement along the fault with a low slip rate that does not generate intense seismic waves. As mining-induced fault-slip generally leads to seismic events with large magnitude and could inflict devastating damage to underground openings (Ortlepp and Stacey 1994; Blake and Hedley 2003; Ortlepp 2000; Hedley 1992; Lizurek et al. 2015; Alber and Fritschen 2011), the proper evaluation of risk associated with mining-induced fault-slip is crucial not only for the safety of mine workers, but also for steady production. Mining-induced fault-slip has also been an important topic in the field of geophysics as investigations

✉ Atsushi Sainoki
atsushi_sainoki@kumamoto-u.ac.jp

¹ International Research Organization for Advanced Science and Technology, Kumamoto University, Kumamoto, Japan

² Department of Mining and Materials Engineering, McGill University, Montreal, Canada

³ Vale Canada Ltd, Vale Ontario Operation, Sudbury, Canada

of microseismic activities in underground mines provide useful insight into the physical phenomena pertaining to slip movement of geological structures (McGarr 1994; Urbancic and Trifu 1998; Yabe et al. 2015; Naoi et al. 2015; McGarr 1991; Gibowicz and Kijko 1994). Hence, in the contexts of geophysics and rock mechanics for deep underground mines, extensive research has been conducted with numerical modelling, laboratory experiments, and field monitoring for a better understanding of seismic events induced by fault-slip.

Numerical modelling and microseismic monitoring have been widely employed in order to understand the mechanism of mining-induced fault-slip and evaluate its risk in response to mining activity. Specifically, when the numerical modelling approach is taken, the following two aspects are mainly focused on: stress state (Alber and Fritschen 2011; Alber et al. 2009) and shear displacement (Sjöberg et al. 2012; Hofmann and Scheepers 2011). The studies (Ziegler et al. 2015) compute the difference between the shear stress acting on a failure plane and the maximum shear strength determined by a failure criterion. Variation corresponds to the change in the risk for fault-slip, while its absolute value indicates the potential for fault-slip to occur. The ratio of the shear stress to the maximum shear strength is also employed for the assessment of fault-slip potential (Ziegler et al. 2015; Alber et al. 2009). It is occasionally reported that the shear stress level computed from a numerical model is insufficient for slip to take place (Ziegler et al. 2015) despite the actual occurrence of fault-slip. In such a case, back analysis is performed. Alber and Fritschen (2011) back-calculate the friction angle of a slip plane, assuming that fault-slip occurred along a fault with slickenside. Sainoki and Mitri (2016) numerically demonstrate that the strength heterogeneity of a shear zone contributes to the generation of high fault-slip potential. When considering the shear displacement of mining-induced fault-slip, seismic moment is commonly computed (Hofmann and Scheepers 2011; Sjöberg et al. 2012; Potvin et al. 2010), as the numerically computed seismic moment can be quantitatively compared with that estimated from wave forms recorded by microseismic-monitoring systems. Hofmann and Scheepers (2011) and Sainoki and Mitri (2016) focus on major seismic events and perform back analysis to simulate a seismic event with seismic moment comparable to the one estimated from wave form recordings, while Sjöberg et al. (2012) and Potvin et al. (2010) compute cumulative seismic moment for the entire geological structures during a relatively long period of time as the indicator of seismic activity. In the study, Sjöberg et al. (2012) mention the importance of distinguishing seismic slip from aseismic slip because shear displacements taking place along geological discontinuities do not necessarily lead to the release

of large amounts of seismic energy, indicating that the computed cumulative seismic moment with respect to the proposed mining sequence is considered conservative.

In fact, there are several studies in which faults are not the direct cause of major seismic events. In such cases, fault shear movements contribute to the development of stress concentration in burst-prone rockmass. White and Whyatt (1999) examined seismicity and rockburst damage in the Lucky Friday Mine and deduced that slip movements along bedding planes in the stope sidewall caused an increase in the ambient stress and added energy, which contributed to the occurrence of rockbursts in the vicinity of the stope. Importantly, it is mentioned that the stress increase due to the slip movements played more crucial role in the occurrence of rockbursts at the Lucky Friday Mine than the slip movement itself and its ability to generate seismic waves. The seismic activities and their relation to mining activities at the Creighton mine in Sudbury, Canada were investigated with numerical analysis and microseismic-monitoring systems (Snelling et al. 2013). It is reported that no clear correlation was found between locations of seismic events and geological structures. It can be postulated then that aseismic deformations of the geological structures induced stress changes in the surrounding rockmass, thus contributing to the occurrence of seismic events. Naoi et al. (2015) detected extremely small microseismic events with M_w down to -4 using advanced microseismic-monitoring system employing acoustic emission sensors. The detected events are regarded as steady on-fault seismicity caused by significantly small amount of slip movements along the fault. One of the possibilities that the authors consider as the cause of the microseismicity is shearing of microasperities due to macroscopic creep behaviour of the fault, i.e. stable slip.

Alternatively, microseismic activities on the fault are occasionally precursors to major seismic events (Trifu and Urbancic 1996; Naoi et al. 2015; Yabe et al. 2015; Zhang et al. 2015). Yabe et al. (2015) examine foreshock activities in the ultra-deep gold mine with the seismic-monitoring system employing acoustic emission sensors and confirm with core samples collected from the rupture plane of a main shock that microseismic activities prior to the major rupture take place in inherently weak patches. The authors conclude that the microscopic failures eventually generate spatially distributed stress concentrations that interact with each other at the final stage before the main shock. Zhang et al. (2015) examined microseismic event rate, released energy, and b-value based on microseismic activities before a large seismic event took place in a crown pillar. The study showed that during fault propagation, the microseismic event rate decreased compared to that during fault movement, while released energy increased nonlinearly, resulting in a decrease in b-value. The authors

conclude that microseismic activity change is associated with the occurrence of a major event.

Previous studies suggest the presence of two types of faults. The first type is the fault that produces intense seismic events entailing the release of large amount of elastic strain energy. The large events take place when the quasi-static evolution of fractures due to the microseismic events turns to uncontrolled, violent failure (Lockner et al. 1991; Trifu and Urbancic 1996). Another type is the one in which there are no major seismic activities. In such a case, microseismic activities related to stable slips with comparatively low fault-slip rates predominantly occur. Generally, seismic moment computed from numerical analyses is regarded as the indicator of intensity of seismicity without a doubt. However, the presence of a fault with aseismic, stable slip movements brings up questions regarding the validity of the exclusive use of seismic moment as the indicator, since it may lead to unnecessary precautions. Evaluating and assessing fault-slip rate may be required to characterize such aseismic fault-slip. The present study focuses on aseismic fault-slip, and a case study is undertaken for a fault in a deep hard rock mine in Canada. Using a 3D model encompassing major geological structures in the region of interest, numerical analyses are performed. The stress state and shear movement of the fault in response to the past mining activities are examined with static and dynamic analyses. The results are compared with seismic events recorded by the mine's seismic-monitoring system.

2 Copper Cliff Mine

The case study is conducted for the Copper Cliff Mine located in Sudbury, Canada. In the present study, a 3D orebody-wide model encompassing geological structures in the area of interest is constructed with Rhino (McNeel & Associates 2015), Kubrix (Itasca Consulting Group 2013) and FLAC 3D (Itasca 2009).

2.1 3D Orebody-Wide Model Representing Main Geological Structures in Area of Interest

Figure 1 shows the 3D orebody-wide model, which encompasses the major geological structures in the region of interest, i.e. the 100 and 900 Orebodies, dykes, and 900 Orebody Cross fault; the remaining part is host rock. In the model, the y- and x-directions correspond to north and east, respectively. To adequately accommodate the main geological structures and mitigate the effect of the outer boundaries on the stress state in the area of interest, the outer boundaries are constructed at least 300 m away from any locations of the geological structures. Specifically, the

top boundary of the model corresponds to 500 Level (152 m below the surface), and the bottom boundary is situated on 8200 Level (2500 m below the surface); the width and length are 1194 and 1930 m, respectively. Dense meshes are generated near these geological structures in order to simulate stress distribution as accurately as possible, while the domain is discretized with coarse meshes near the outer boundaries. Consequently, the total numbers of zones and grid points in the model are 6,370,802 and 1,093,934, respectively, which consumes 8 GB memory.

2.2 Mineralogical Characteristics of Geological Structures in the Area of Interest

The 100 and 900 Orebodies (OB) in Fig. 1 are pipe-shaped and sub-parallel in close proximity to each other, extending over 1200 m vertically but only 90–150 m horizontally. The 100 OB consists of inclusions of massive-to-heavily disseminated sulphide mineralization with a sharp contact against the surrounding waste rock, while the 900 OB is composed mostly of erratic sulphide stringers and lenses with some disseminated mineralization. The main host rock for the orebodies is predominantly massive quartz diorite, which is primarily composed of amphibole, biotite and chlorite. The fault generally dips at 45° to the north and consists of strongly sheared, black biotite schist and minor carbonate mud gouge within its boundaries. The width of the fault varies from 3.6 to 4.6 metres, and it has created very blocky, semi-vertical joint systems up to 6 metres on each side. The dykes are composed of olivine and quartz diabase and intersect with the 100 and 900 orebodies.

2.3 Stope Extraction Sequence Employed in the Copper Cliff Mine

Figure 2 depicts only the orebodies and the fault along with the stope extraction sequence that was employed at the mine. As the orebody geometry above 4200 Level was delineated with wire frames created by cavity monitoring after extracting stopes, the boundaries between stopes on each level are not accurately constructed. It is to be noted, however, that the purpose of the present study is to investigate the effect of the long-term mining activities in the orebodies on the fault. As shown in the model parametric study with respect to the distance between a steeply dipping tabular orebody and a fault, (Sainoki and Mitri 2014b), a large amount of ore extraction is required to reactivate the fault. Thus, the effect of extraction of each stope is ignorable.

As shown in Fig. 2, stopes above 3000 Level are extracted first as per the mining sequence in accordance with a sublevel stoping method. Afterwards, the second and the third mining fronts advance upward from 3500 Level

Fig. 1 3D orebody-wide model encompassing major geological structures in the area of interest

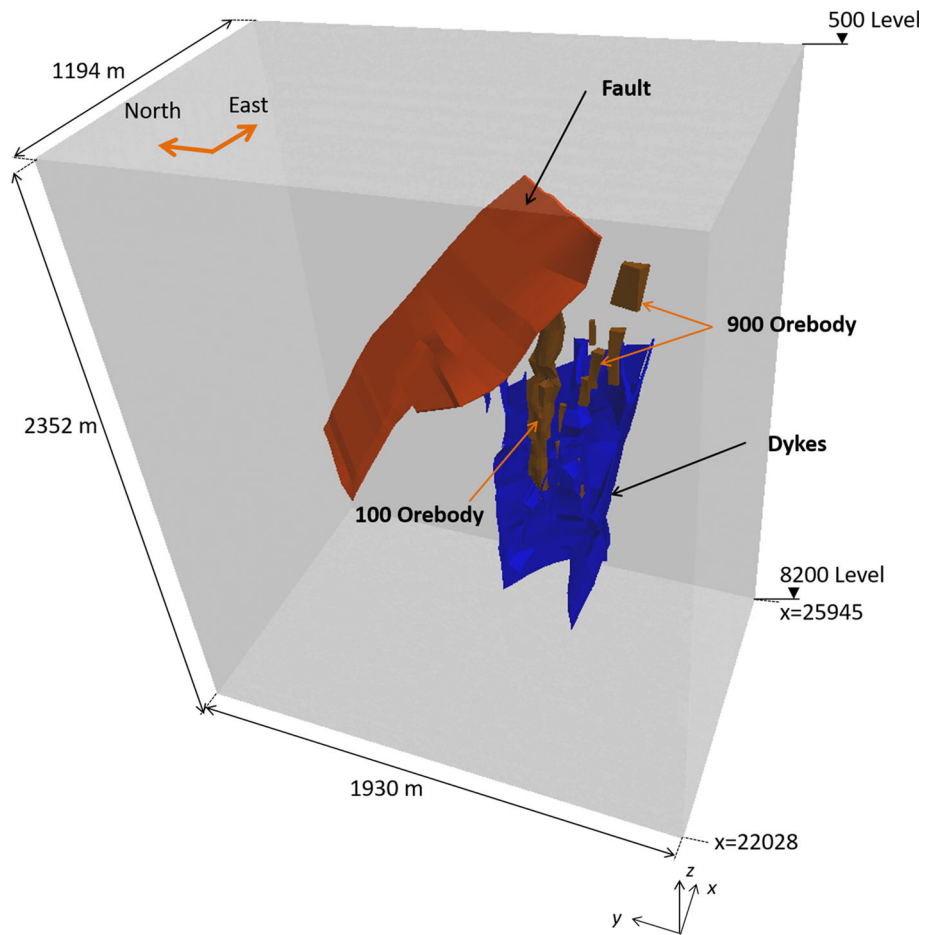
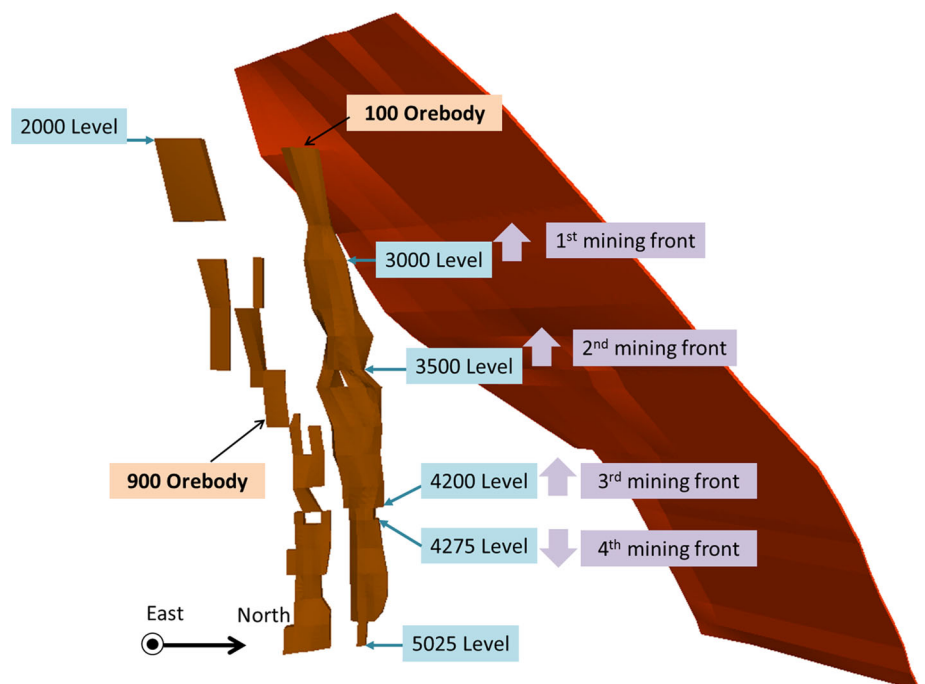


Fig. 2 Mining sequence and positional relation between the orebody and the fault



and 4200 Level, respectively. In reality, stopes were simultaneously mined out until the end of 2008 during the second and the third mining sequences. However, as described above, boundaries of stopes on the levels during the mining sequences are not accurately modelled. Therefore, the present study does not consider the simultaneous mining; hence, after extracting stopes in accordance with the second mining sequence, the third stope extraction sequence begins, followed by the fourth mining sequence going downward from 4275 Level.

2.4 Numerical Simulation Methods and Model Input Parameters

In the present study, three types of numerical analyses are carried out, namely elastic and elasto-plastic analyses in static conditions and elasto-plastic analysis in dynamic conditions. The elastic analysis is performed for the purpose of estimating the maximum fault-slip potential in the fault, i.e. its excess shear stress (Ryder 1988). For instance, Ziegler et al. (2015) constructed a mine-wide model for the case study of a deep underground gold mine in South Africa. The authors employed the simplest elastic model to evaluate the excess shear stress on a seismic source location. The static, elasto-plastic analysis is intended to simulate the actual deformation of the fault material, i.e. slip movements. It is a common practice to perform elasto-plastic analysis with Hoek and Brown criterion or Mohr–Coulomb failure criterion for the numerical simulation of rockmass behaviour in deep hard rock underground mines (Snelling et al. 2013; Sjöberg et al. 2012). Lastly, the dynamic, elasto-plastic analysis is conducted to help estimate the slip rate, assuming that dynamic shear movements taking place on the fault are due to instantaneous asperity breakage. A similar approach to simulate dynamic fault-slip was adopted in the study (Rutqvist et al. 2013). The results are then used to discuss the potential use of slip rate as an indicator to distinguish aseismic from seismic fault-slip. Table 1 lists deformation moduli and Poisson’s ratios for the rockmasses described in Sect. 2.2. Note that the rockmass rating system developed by Bieniawski (1976) is employed to convert the mechanical properties derived from laboratory experiments to those for the in situ rockmass. For the host rock and orebody, RMR is estimated to

Table 1 Mechanical properties of the rockmasses for elastic analysis

	E_{rockmass} (GPa)	ν	Density (kg/m ³)
Host rock	37.8	0.24	2907
Ore	27.6	0.28	3700
Dyke	60	0.22	2907
Fault material	0.4	0.25	2907

65 with field observation, while RMR of 100 is assumed for the dyke, considering that the dyke is generally massive. For the fault, the conversion is not performed, i.e. the laboratory-derived value is used as an input because the modulus is considered sufficiently low to reflect the characteristic of the fault. Regarding the density, the average value of rock samples collected from the mine is applied to the host rock, dyke and fault material, while the density of ore is calculated with rock samples collected from the orebody.

For the elasto-plastic analyses, Hoek–Brown failure criterion (Hoek et al. 2002) is applied to the host rock, ore, and dyke, with the parameters listed in Table 2 and then corresponding stress corrections are performed when the stress acting on the rockmasses exceeds the failure criterion. In order to calculate the parameter, s , the same RMR used for the calculation of the deformation moduli is applied. As for the parameter, m_i , the values for diorite (Hoek 2007), sulphide (Cai 2010), and diabase (Hoek 2007) are used for the host rock, ore, and dyke, respectively; and the values are converted to m_b for taking into account rockmass strength characteristic (Hoek 2007), using the relationship that $GSI = RMR - 5$. The uniaxial compressive strengths, σ_c , are derived from laboratory experiments.

Regarding the fault material mainly composed of schist, a ubiquitous joint model, which is widely used to simulate slip movements along faults (Cappa and Rutqvist 2011), is applied, and corresponding input parameters are calculated as shown in Table 3. In the table, the cohesion is estimated from the uniaxial compressive strength of 62 MPa derived from a laboratory experiment, using the Hoek–Brown failure criterion with the substitution of $\sigma_3 = 0$ and assuming $GSI = 20$. Note that $m_i = 12$ is assumed for the fault material as it mainly consists of schist (Hoek 2007). The GSI for the fault material is taken from the chart proposed for heterogeneous rockmasses (Marinos and Hoek 2001), based on the field observation that the fault is blocky and considerably sheared. In fact, as can be seen in Fig. 3, the fault is heavily fractured. According to Wyllie

Table 2 Hoek–Brown parameters of the rockmasses

	s	m_i	m_b	σ_c
Host rock	0.012	25	6.0	150
Ore	0.012	24	5.8	150
Dyke	0.57	15	12.5	220

Table 3 Mechanical properties of the fault material

C (MPa)	ϕ (°)	ϕ_d (°)	ψ (°)	σ_T (MPa)
0.24	23.5	20.0	5.9	0.07



Fig. 3 Section of 900 Orebody cross fault intersected between 3400 Level and 3500 Level

(2003), the friction angle of schist varies from 20° to 27° . Hence, the intermediate value of the range is adopted, and dilation angle is set to one-fourth of the friction angle (Hoek and Brown 1997). The tensile strength is estimated from the uniaxial compressive strength taking into account GSI, using the equation proposed by Altindag and Guney (2010). As for the dynamic friction angle, ϕ_d , it is challenging to determine the value because it is dependent upon a number of factors, such as slip rate (Yuan and Prakash 2008), static frictional resistance, slip distance, and state (Dieterich and Kilgore 1996; Ohnaka et al. 1997). A number of studies have shown that the frictional coefficient of a fault surface decreases when dynamic slip takes place (Yuan and Prakash 2008; Dieterich 1979; Okubo and Dieterich 1984), according to which a number of friction laws have been proposed (Ruina 1983; Dieterich and Kilgore 1996; Sainoki and Mitri 2015). It may be true that the frictional coefficient does not decrease instantaneously. However, as mentioned by Kanamori (2001), in the case of shallow earthquakes, the assumption of instantaneous stress drop is acceptable. As a matter of fact, many studies related to mining-induced fault-slip assume instantaneous stress drop. (Hofmann and Scheepers 2011; Sainoki and Mitri 2014a; Sjöberg et al. 2012), although fault-slip magnitude varies depending on the slip-weakening distance (Sainoki and Mitri 2015). As shown in Table 3, the present study assumes 20° as the dynamic friction angle of the fault material. The assumption is made based on previous studies and considering the characteristics of this fault material. Sainoki and Mitri (2016) back-analysed the dynamic friction angle of a fault surface, using peak particle velocity and acceleration of rock recorded by micro-seismic-monitoring system installed in an underground mine. According to the study, the friction angle of a fault in a shear zone decreases from 28° to 20° when fault-slip takes place. Urpi et al. (2016) assumed the kinetic friction

of a fault at 0.448 , which is equivalent to a dynamic friction angle of 24° . Hofmann and Scheepers (2011) back-analysed the residual friction angle at 20° for mining-induced conditions, which is 5° less than the static friction angle of 25° . As it is quite challenging to estimate the kinetic friction of a fault with laboratory experiments, generally the values are assumed or back-analysed. In the present study, the friction angle of the fault material is estimated at 23.5° , which is decreased to 20° for the area undergoing slip during the dynamic analysis. The dynamic friction angle is close to the values used in the previous studies, although the difference between static and kinetic frictions in the present study is slightly smaller compared to some other studies. As the fault material is considerably weak and fractured, it is assumed to exhibit ductile behaviour rather than brittle behaviour associated with shearing of noticeable asperities while it is being sheared. Therefore, it is unconceivable that a large stress drop associated with asperity abrasion would take place.

The use of a ubiquitous joint model is deemed reasonable, considering the fact that the fault is approximately 4 m in width. Hence, it is presumed that the weak fault material affects the stress state within the fault. The ubiquitous joint model simulates slip movements by performing stress corrections with respect to the assumed plane of weakness. The dip angle and dip direction of the weak plane are set to 45° and 315° , respectively, although to be precise, the geometric properties slightly vary from place to place on the fault. As the ubiquitous joint model is employed in order to examine shear movements along the fault, the strength properties of the fault material that are not related to the slip behaviour are determined so that shear failure takes place only along the prescribed plane of weakness.

3 Calibration of In-Situ Stress State for 3D Orebody-Wide Model

Before performing the elastic and elasto-plastic analyses, stresses to be applied to the model outer boundaries are calibrated (Shnorhokian et al. 2014). For the calibration, equations used for the mine are employed that describe the relation between mining depth and in situ stress regimes. The relation is almost identical to that proposed by Herget (1987) and is expressed as follows:

$$\sigma_{H_{\max}}^o = 0.0407 \times D + 10.35 \quad (1)$$

$$\sigma_{H_{\min}}^o = 0.0326 \times D + 8.69 \quad (2)$$

$$\sigma_v^o = 0.029 \times D \quad (3)$$

where D represents a mining depth in metres. The orientation of the maximum horizontal stress corresponds to the

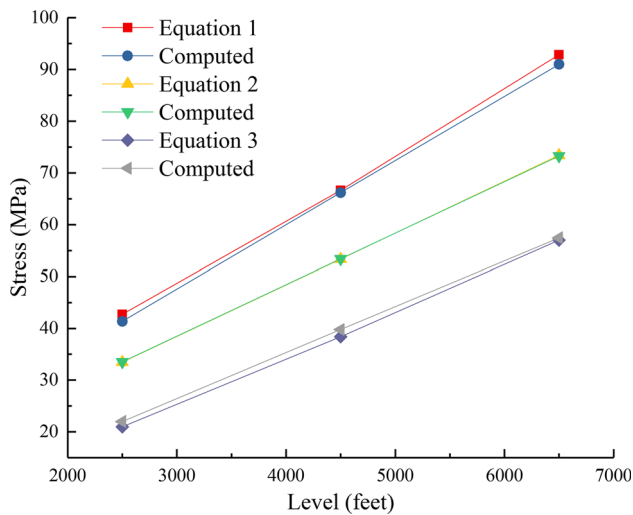


Fig. 4 Stresses computed from a numerical analysis with calibrated boundary tractions and derived from the equations at the three locations

x-direction in Fig. 1, that is, the minimum horizontal stress acts in the y-direction. Note that the unit of stresses calculated from the equation is MPa.

The calibration is carried out based on three points located on 2500, 4500 and 6500 Level. The three points are situated sufficiently away from the geological structures shown in Fig. 1 such that stresses at the points represent in situ stresses that are not influenced by the geological structures. The boundary tractions are adjusted until the stresses at the three points adequately agree with those calculated from Eqs. (1) to (3). Figure 4 shows stresses computed from a numerical analysis using the calibrated boundary tractions and derived from the equations. It is found from the figure that the stresses are almost identical. Note that the calibrated stresses are used for both elastic and elasto-plastic analyses because the pre-mining stress state in the elastic analysis is the same as that in the elasto-plastic analysis, in regions away from the geological structures. The reason why stresses are applied to the boundary instead of each zone in the model is to reproduce the influence of rockmass stiffness on the in situ stress state, i.e. stiff rockmass such as dyke generally carries high stress, while stress state is relatively low in weak rockmass (Bewick et al. 2009).

4 Result of Elastic Analysis

Based on the results obtained from the elastic analysis, potential for fault-slip is assessed with respect to each stage during the mining sequence. Two types of stress-based evaluation criterion are employed, based on the classical Mohr–Coulomb criterion as follows:

$$CFS_1 = \sigma_1 - \sigma_{max} = \sigma_1 - \left(\sigma_c + \frac{1 + \sin \phi}{1 - \sin \phi} \sigma_3 \right) \quad (4)$$

$$CFS_2 = \tau - \tau_{max} = \tau - (C + \sigma_n \tan \phi) \quad (5)$$

where σ_1 and σ_3 are the maximum and minimum compressive stresses, respectively, and τ is the shear stress acting along the fault, which is computed assuming the dip angle of 45° and the dip direction of 315° . Thus, CFS_1 (Coulomb failure stress) represents potential for failure (slip movement) with respect to the plane of principal stresses, while CFS_2 gives potential for failure along the fault plane with the dip angle and dip direction. As can be seen in Fig. 3, the fault considered in the present study is thick and strongly discontinuous, indicating that failure can occur in any direction within the fault. Therefore, considering only the general dip and dip direction is insufficient in order to assess the potential for slip movements in the fault, leading to the use of two evaluation criteria.

4.1 CFS (Coulomb failure stress) at Pre-mining Stress State

Figure 5 shows potential for fault-slip computed with the two evaluation criteria. It is found from Fig. 5a that CFS_1 takes positive values in almost the entire fault, and the negative fault-slip potential takes place only in a small region near the top boundary, implying that the negative value may be due to the boundary effect. The important implication of these results is that the fault material had undergone shear failure at the pre-mining stage, because the positive value of CFS_1 indicates that the stresses had reached the failure envelope. It appears that CFS_1 gradually increases with mining depth, albeit anomalies with noticeably high CFS_1 as much as 20 MPa occur near the centre of the fault, as shown in Fig. 5a. It is speculated that the anomalies are attributed to stress concentrations due to the fault geometry. It is to be noted that the positive CFS_1 in almost the entire fault at the pre-mining stage suggests the intense failure of fault materials, which is in agreement with the geological features of the fault, i.e. strongly sheared and fractured.

It is quite interesting that characteristics of CFS_2 shown in Fig. 5b differ completely from those in Fig. 5a. The most noticeable discrepancy is that CFS_2 has negative values in large areas within the fault. Positive values of CFS_2 are found only at the upper left area and along the boundary. The positive CFS_2 along the boundary is possibly attributed to the stress concentrations that are essentially similar to the phenomenon taking place at a crack tip (Fischer-Cripps and Mustafaev 2000) because the fault material has the significantly lower elastic modulus than that of the host rock. Another important aspect to be

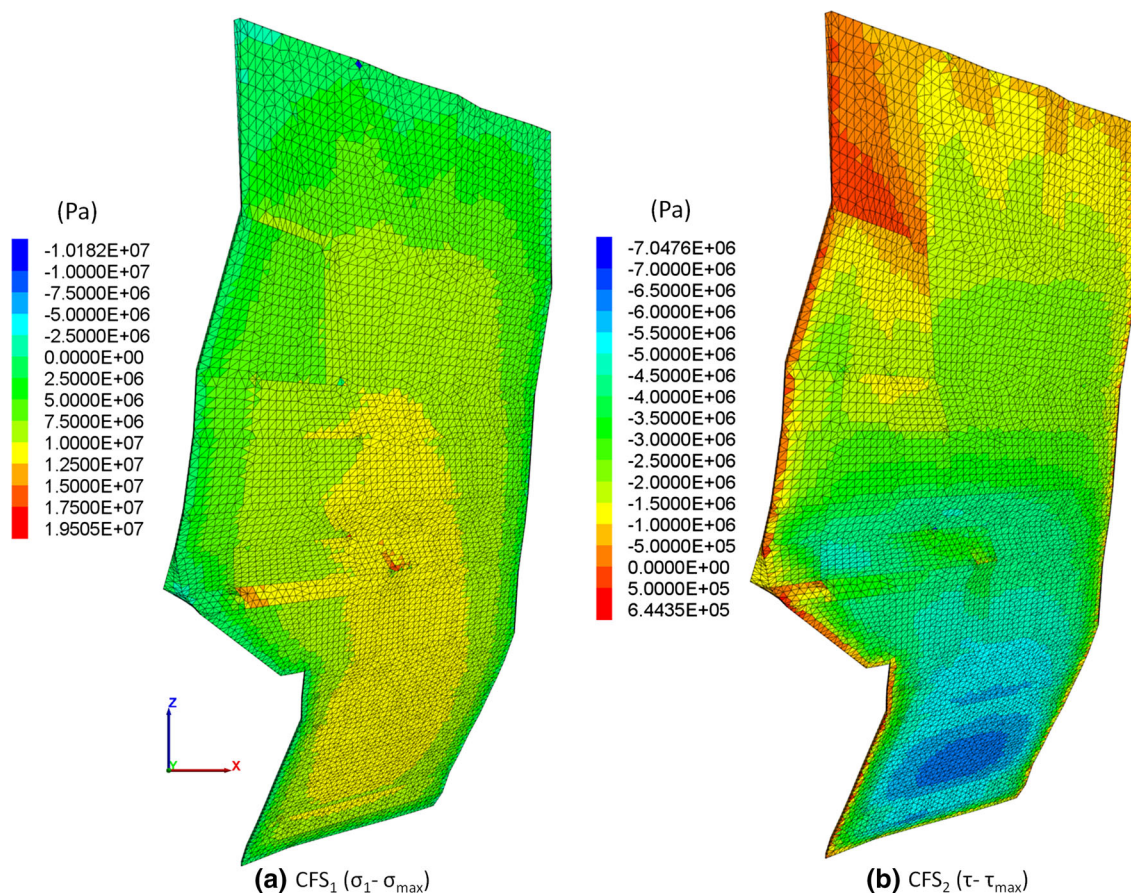


Fig. 5 Estimating the potential for fault-slip using Eqs. (4) and (5)

discussed is that CFS_2 decreases with mining depth, meaning that the possibility of fault-slip taking place decreases with increasing mining depth. The decrease in CFS_2 with mining depth is unreasonable when considering the relation between the orientations of the maximum horizontal stress and the fault, that is, the increase in the maximum horizontal stress should contribute to an increase in CFS_2 . The discussion leads to the assumption that the in situ stresses within the fault are rotated. To verify this assumption, the stress orientations are examined and shown in Fig. 6. The figure depicts stress orientations within the fault on 4200 Level. As can be seen in the figure, in the host rock, the orientation of the maximum stress is sub-parallel to the x-axis, whereas the orientation is rotated within the fault, so that the maximum stress acts perpendicularly against the fault. Hence, the maximum compressive stress in the fault gives rise to clamping force, which directly contributes to an increase in τ_{max} rather than an increase in the shear stress acting along the fault. Therefore, considering the rotation of the maximum stress within the fault, the results shown in Fig. 5b are

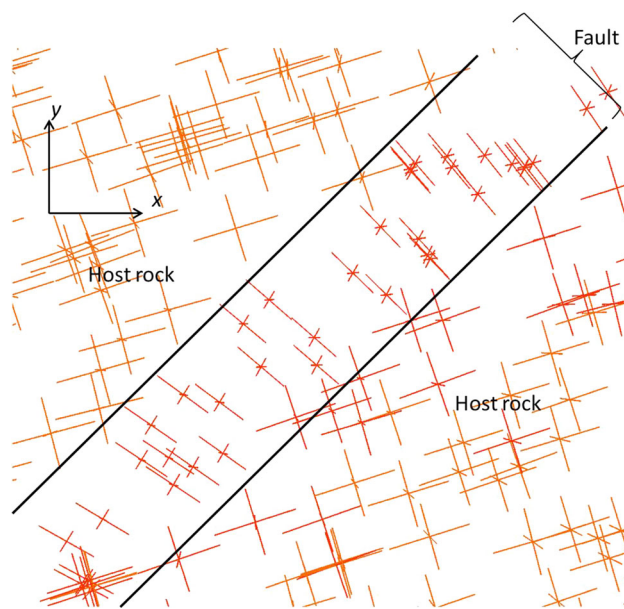


Fig. 6 Stress orientation within the fault in the x-y plane on 4200 Level

reasonable. Importantly, the result implies that the stress rotation might be an important aspect to evaluate potential for fault-slip, especially in such a case where faults have thick, weak fault zones. It is assumed that if the fault were similar to a rock joint in the absence of a thick fault zone, the stress rotation within the fault would be insignificant. Accordingly, the ambient stresses in the surrounding rockmass would be almost the same as stresses acting on the fault. As such, the interlocking of fault surface asperities plays a key role in determining the strength of the fault and thus the generation of fault-slip (Barton 1973; Sainoki and Mitri 2014a; Bandis et al. 1983). The comparison between CFS_1 and CFS_2 suggests the need to employ both criteria to comprehend the state of fault materials. The exclusive use of one criterion without the other may lead to improper estimation of fault-slip potential in a case where the fault has thick, weak shear zones.

4.2 Change in CFS During the Mining Sequences

Figure 7 depicts increments of CFS_1 for each stage of the mining sequences illustrated in Fig. 2. For instance, Fig. 7b presents the increase in CFS_1 from the stress state after completing the first mining stage (3000 Level to 2000 Level) to that after completing the second mining stage (3500 Level to 3000 Level). In Fig. 7, the backfilled stopes as well as unmined orebodies are also shown to clarify the relation between extracted stopes and change in CFS_1 . It is found that regions where CFS_1 increases are not limited by the proximity to stopes extracted during the mining sequences. For instance, as can be seen in Fig. 7a, an increase in CFS_1 takes place not only in an extensive area above 3000 Level but also in some areas near 3500 Level as a result of the first mining stage extracting stopes from 3000 Level to 2000 Level. The increase in CFS_1 indicates that the possibility of seismic events taking place rises in the areas. Conversely, CFS_1 decreases in the lower part of the fault below 3000 Level, as well as in some areas near the extracted stopes during the mining sequence. Likewise, CFS_1 increases in extensive areas during the subsequent mining sequences while showing the most intensive rise near the extracted stopes. It is to be noted that CFS_1 takes positive values in almost the entire fault at the pre-mining stage. It means that a slight increase in CFS_1 can cause shear-failure-induced plastic deformational behaviour to the fault material, resulting in a large relative shear displacement, although the produced displacements are not parallel to the fault because the orientation of the maximum stress acting on the fault is perpendicular to the fault, as shown in Fig. 6. In terms of the magnitude of CFS_1 change, the influence of the mining activities becomes insignificant as the mining sequence proceeds. This is

because the distance between the orebodies and the fault increases with mining depth as shown in Fig. 2. The maximum increase in CFS_1 due to the first mining sequence is as much as 0.33 MPa according to Fig. 7a, and it then decreases to 0.06 MPa when the fourth mining sequence is completed, referring to Fig. 7d.

Figure 8 shows the change in CFS_2 for the same stages as those in Fig. 7. For example, Fig. 8a presents the increase in CFS_2 from the stress state at the pre-mining stage to that after completing the first mining stage (3000 to 2000 Level). It is interesting that CFS_2 varies within the fault in quite a different way from CFS_1 . For instance, during the second mining stage, CFS_1 particularly decreases in the region between 3500 Level and 3000 Level, as can be seen in Fig. 7b, whereas CFS_2 does not decrease in this region, according to Fig. 8b. Similar phenomena occur, to some extent, during the other mining stages. Another important aspect to be discussed is that an increase in CFS_2 does not necessarily cause plastic deformations in the fault material, because CFS_2 is generally negative at the pre-mining stage, the exception being the small region around 2000 Level, as shown in Fig. 5b. Hence, in this fault, it can be concluded that a large shear displacement along the fault is unlikely to occur. Areas near the extracted stopes on 2000 Level have the highest possibility of slip movements along the fault to take place. However, it should be noted that shear displacements due to shear failure, which does not develop along the fault, can occur at any locations in the fault, as discussed above, due to the large thicknesses of the fault.

5 Results and Discussion for Static, Elasto-Plastic Analysis

As mentioned in the previous sections, an elasto-plastic analysis is performed in order to simulate slip movements along the fault by means of the ubiquitous joint model. Note that the simulation procedure for the elasto-plastic analysis is exactly the same as that for the elastic analysis. As discussed in the previous section with Figs. 5 and 8, shear movements along the fault are most likely to occur in the fault on 2000 Level during the first mining sequence. Thus, the shear displacement increments induced by stope extraction during the mining stage are of particular importance. Figure 9 shows the maximum shear displacement increments from the pre-mining stage to the end of the first mining stage. As discussed in Sect. 2.4, the fault material undergoes shear failure only along the prescribed plane of weakness, using the ubiquitous joint model. In this way, shear movements along the fault that are not affected by failure in other directions can be evaluated.

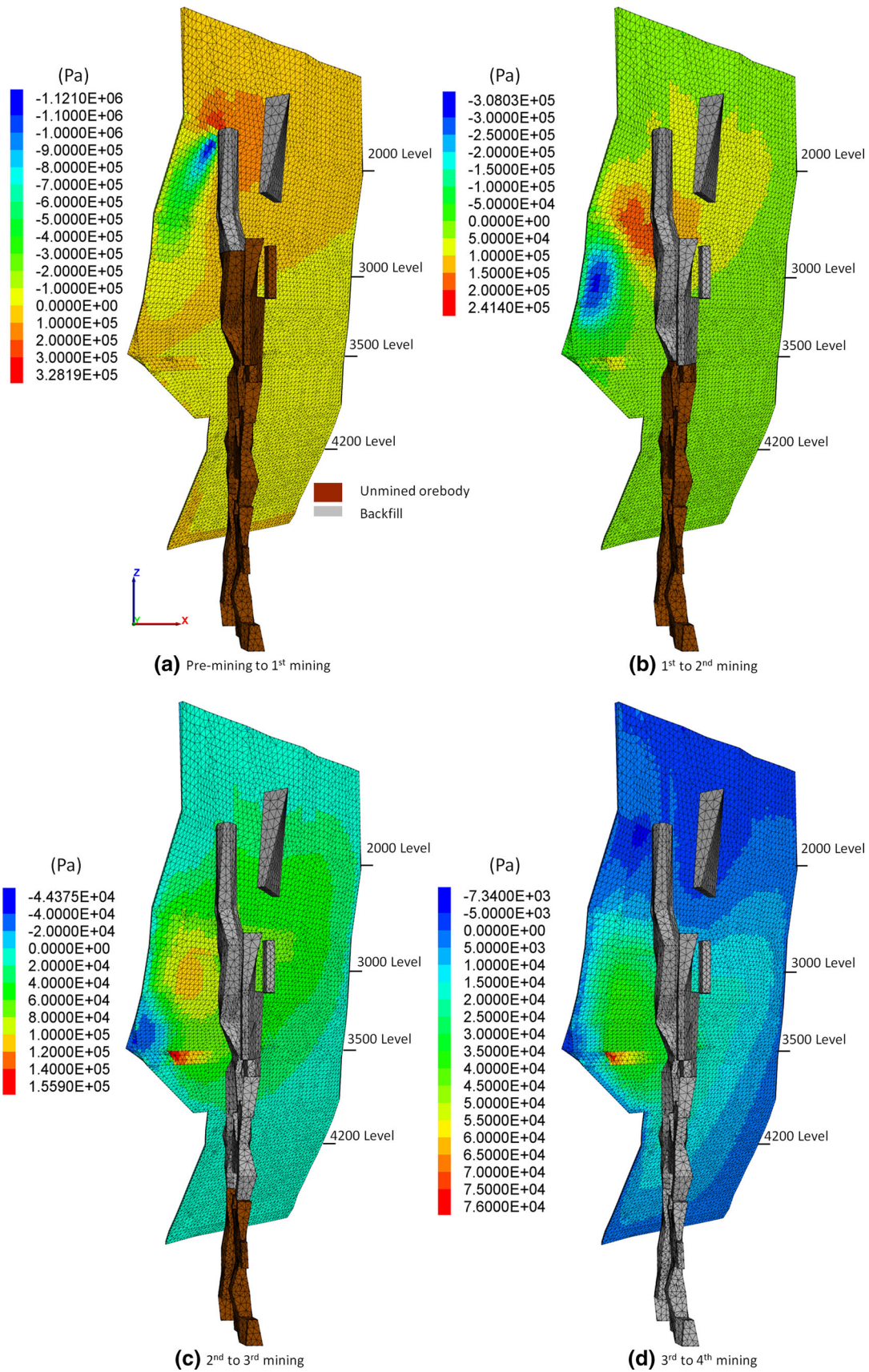


Fig. 7 Changes in CFS-1 during the mining sequences shown in Fig. 2

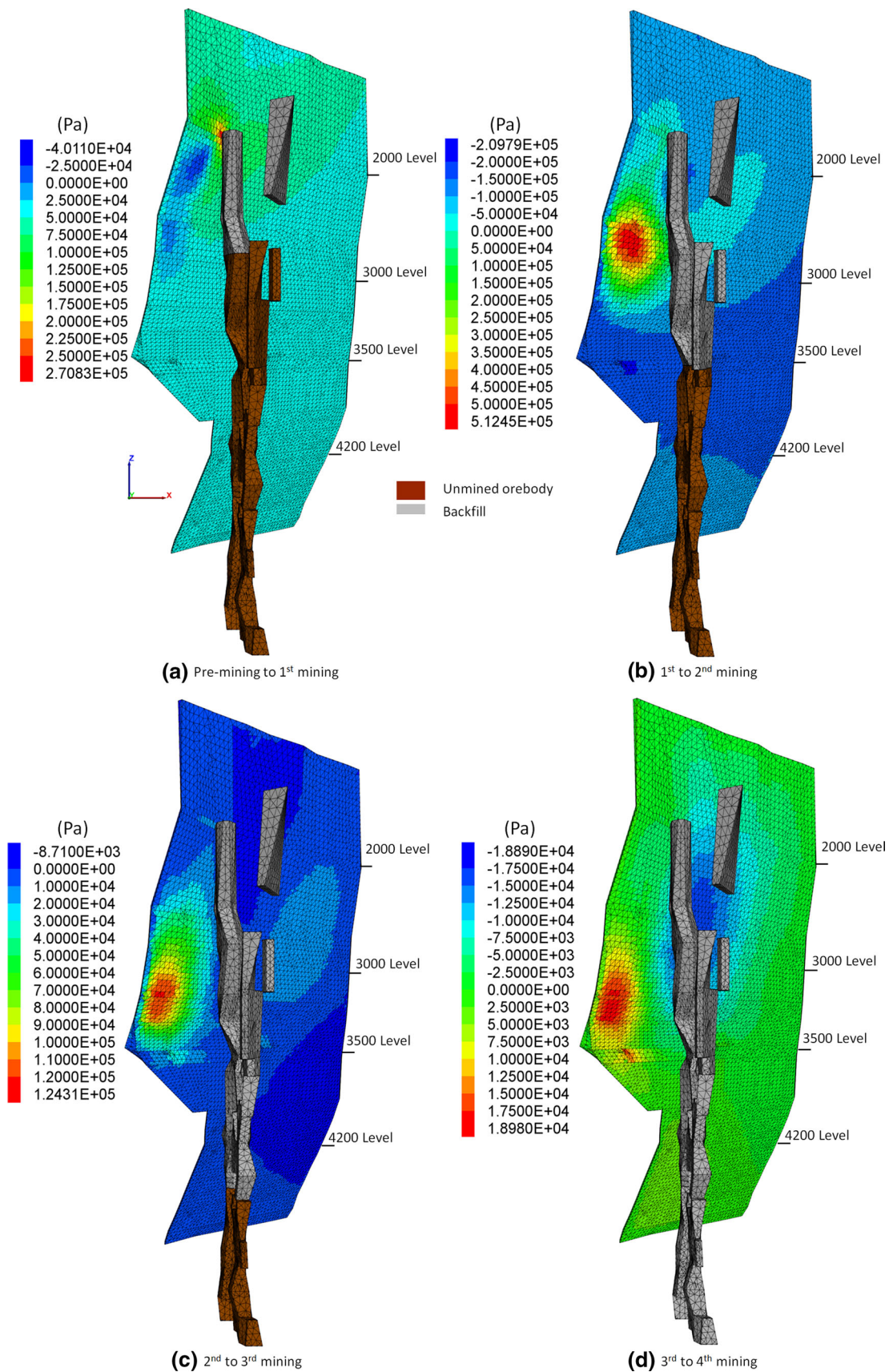


Fig. 8 Changes in CFS-2 during the mining sequences shown in Fig. 2

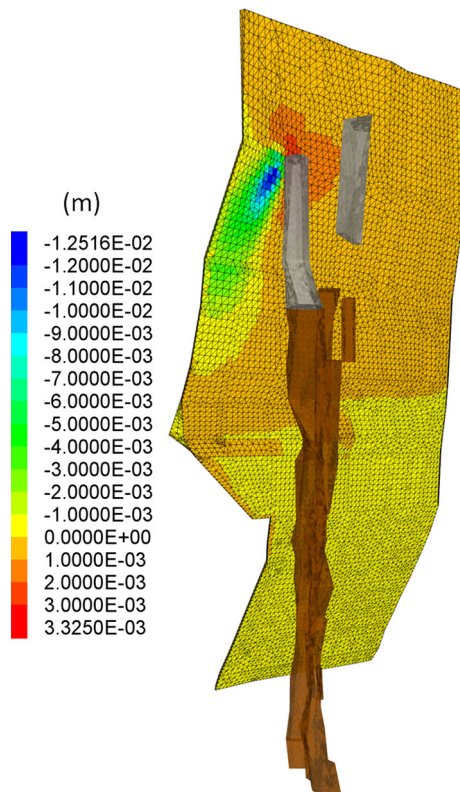


Fig. 9 Maximum shear displacement increments induced by mining activities during the first mining stage

It is found from Fig. 9 that the increments of shear displacements along the fault are insignificant and no more than 3 mm, even near the extracted stopes. The magnitude of the maximum shear displacement increment is considerably smaller, compared to the case where mining activity with a sublevel stoping method is simulated considering its influence on a nearby fault (Sainoki and Mitri 2014a). Sainoki and Mitri (2014a) simulate fault-slip taking place along a fault running parallel to a steeply dipping, tabular orebody in a deep hard rock mine and demonstrate that the maximum shear displacement can exceed 16 cm when the friction angle of the fault is low. The volume of stopes extracted during one mining stage in the study is 66,000 m³, while in the present study the total volume of stopes extracted during the first mining stage is 590,000 m³. In spite of the larger volume of extracted stopes in the present study, the shear displacements shown in Fig. 9 are significantly smaller. The following two aspects help us understand the results: the distance between the fault and orebody, and the low stress environment in the fault. First, regarding the distance, it is found from Fig. 2 that although the stope on 2000 Level is located in close proximity to the fault, the distance increases with mining depth. Indeed, the stope on 3000 Level, which is extracted at the beginning of the first mining sequence, is

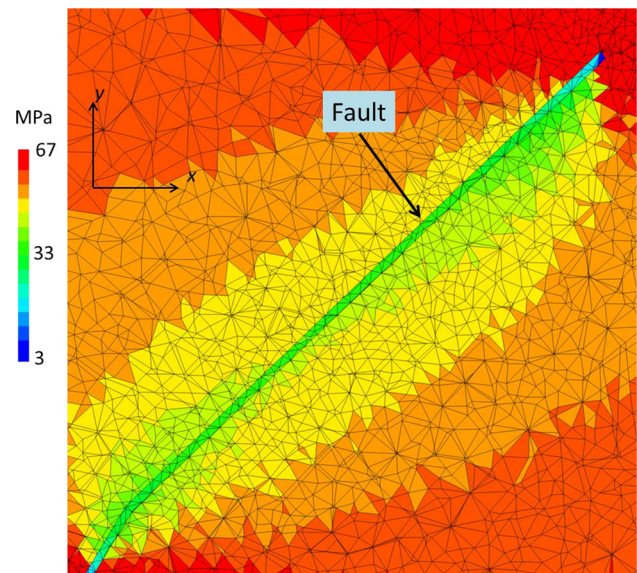


Fig. 10 Maximum compressive stress near and within the fault on 4200 Level

located 130 m away from the fault. In the case analysed by Sainoki and Mitri (2014b), fault-slip does not occur when the distance between the fault and orebody is more than 40 m. Thus, although the volume of extracted stopes during the first mining stage is large, the stope extraction is assumed to have a lesser influence on the fault, compared to the case (Sainoki and Mitri 2014a) where the distance between the orebody and the fault is 30 m. Regarding the stress environment, an example of the maximum compressive stress near the fault on 4200 Level is shown in Fig. 10. The figure shows that the fault material carries lower stresses than the surrounding host rock because of the low stiffness of the fault material, which is approximately 1% of that of the host rock. At a rough estimate from Fig. 10, the maximum compressive stress within the fault is one-half of that of host rock situated sufficiently away from the fault. It is concluded that these two aspects predominantly contribute to the small shear movements along the fault, and the result indicates that the possibility of large seismic event taking place on this fault is minor. Thus, seismic events that may occur on this fault would be characterized as the aggregation of small seismic events due to the low stress environment and the minor influence of mining-induced stress.

6 Results and Discussion for Elasto-Plastic Analysis Under Dynamic Conditions

The elasto-plastic, static analysis shows that the potential for fault-slip is positive on the fault. The next step is to estimate the severity of the seismic activities due to fault-

slip. To do so, the present study performs a dynamic analysis to estimate slip rate, which pertains to the near-field peak particle velocity of a rockmass representing the severity of ground motions. There are numerical and empirical approaches for the estimation of fault-slip rate (McGarr 2002; Cappa and Rutqvist 2012). The present study adopts the numerical approach as the stress drop caused by the transition from static to dynamic frictional resistance can be explicitly taken into consideration in the numerical simulation, while the empirical approach relies on selecting a value from several past case studies (Hedley 1992; McGarr 2002).

6.1 Procedure of Dynamic Analysis

As discussed in previous sections, the largest slip movements along the fault are most likely to occur during the first mining stage. Thus, the dynamic, elasto-plastic analysis is performed based on the stress state immediately after the first mining stage, i.e. the initial stress state for the dynamic analysis is obtained from the static, elasto-plastic analysis. After completing the stope extraction of the first mining state, the boundary conditions are changed to the viscous boundary condition (Lysmer and Kuhlemeyer 1969), which prevents seismic waves caused by fault-slip from reflecting on the model outer boundaries. In order to consider the attenuation of kinetic energy, local damping, which is embedded in FLAC3D, is employed, assuming 5% of critical damping. According to (ABAQUS 2003), the damping coefficient of rock ranges from 2 to 5%, which was employed in some studies (Van Gool 2007). Considering the estimate, the present study assumes 5% for the damping coefficient of the rockmass. Detailed description of the damping system is found in the FLAC3D user manual. Although the local damping system cannot capture energy loss accurately when the stress waveforms are complex, the damping system is deemed sufficient as the damping mainly affects the attenuation and propagation of stress waves, which are not the focus of the present study. A timestep used in the dynamic analysis is automatically optimized based on the volume of each zone of the model, P-wave velocity derived from the rockmass mechanical properties, and the face area of each zone. The actual time step used during the dynamic analysis is approximately 4.9×10^{-7} s.

At the beginning of the dynamic analysis, the stress state in the fault is examined, and for the area where the difference between the maximum shear strength and the maximum shear stress along the fault is less than 1 MPa, the cohesion and friction angle of the fault material are set to zero and the dynamic friction angle, respectively, as listed in Table 3. Fault-slip is driven by the excess shear stress (Ryder 1988) defined as the difference between static

and kinetic friction laws. In reality, the instantaneous decrease in friction angle does not occur; the change from static to the dynamic friction is associated with an increase in a shear displacement along the fault (Ida 1972; Okubo and Dieterich 1984), which is generally referred to as a slip-weakening distance. Slip rate increases with a decrease in the slip-weakening distance, since the shear stress acting on the fault is instantaneously released when the slip-weakening distance approaches zero. The instantaneous change from static to dynamic friction law corresponds to a zero slip-weakening distance. Hence, it should be noted that the slip rate obtained from the dynamic analysis in the present study is the maximum value that can occur under the stress state.

6.2 Near-Field Ground Motion (a Half of Slip Rate) Estimated from Dynamic Analysis

Figure 11 shows the maximum slip rate of the fault patches during the dynamic analysis. The maximum slip rate is computed as twice near-field ground motion, i.e. the peak particle velocity of grid points (McGarr 1991). As expected from the stress state and shear displacements shown in Figs. 5 and 9, the region where shear movements take place during the dynamic analysis is limited to around 2000 Level. More importantly, Fig. 11 clearly shows that the maximum slip rate is no more than 0.3 m/s, which is comparable to the lowest slip rate among mine tremors

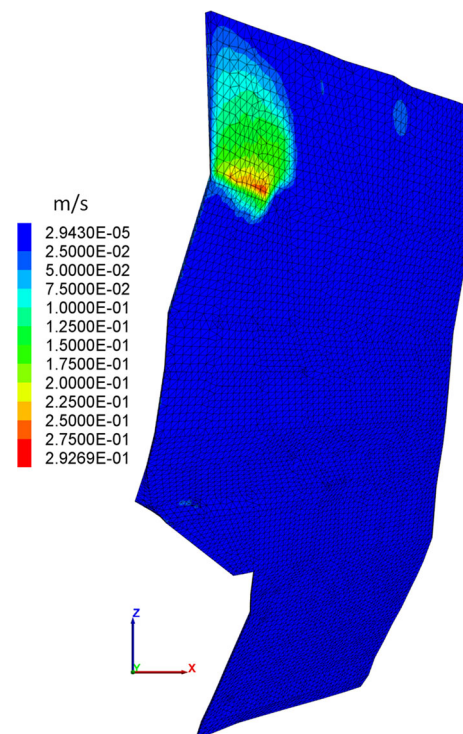


Fig. 11 Maximum particle velocity within the fault during fault-slip

reported by McGarr (1991). Furthermore, as discussed above, the simulation procedure for dynamic fault-slip adopted in the present study gives the highest slip rate that can be induced in the simulated stress regimes because of the instantaneous stress drop. Thus, slip rates during fault-slip would be less than the simulated values shown in Fig. 11 when fault-slip occurs in dynamic conditions. In addition, the peak particle velocity is far below the threshold of peak particle velocity that causes severe damage to rockmass (Hedley 1992; Brinkmann 1987). These results imply that the seismic activity of the fault is considerably low.

7 Validation of Results Obtained from the Static and Dynamic Analyses with In Situ Monitoring of Seismicity in the Copper Cliff Mine

The results obtained from the static and dynamic analyses strongly suggest that the possibility of large, intense seismic events taking place along the fault ought to be low. To validate the results, actual seismic events that took place at the Copper Cliff Mine are investigated. The Copper Cliff Mine is equipped with seismic-monitoring systems

composed of 44 accelerometers including both the uniaxial and triaxial sensors to detect seismic events and develop a microseismic database, which can be utilized for improving the safety of working conditions. The seismic wave forms recorded with the sensors are analysed, using ESG software (ESG 2011), and then the source location and seismic source parameters such as seismic moment and seismically released energy are estimated. The possible error with respect to the location of seismic events ranges from 10 feet (3 m) to 50 feet (15 m).

7.1 Comparison with Large Seismic Events

Figure 12 shows locations of relatively large seismic events with $M_w > 0.1$ that occurred during the period of time from 2006 to 2014. During this period, 39 large seismic events took place near the geological structures that are the focus of the present study, with magnitudes ranging from 0.1 to 3.8, as can be seen in the figure. It is to be noticed from the figure that major seismic events predominantly took place near the orebodies, especially between 4200 Level and 3500 Level. Indeed, 87% of those seismic events are located in these regions. Only one of them took place near the fault or within the fault. Herein,

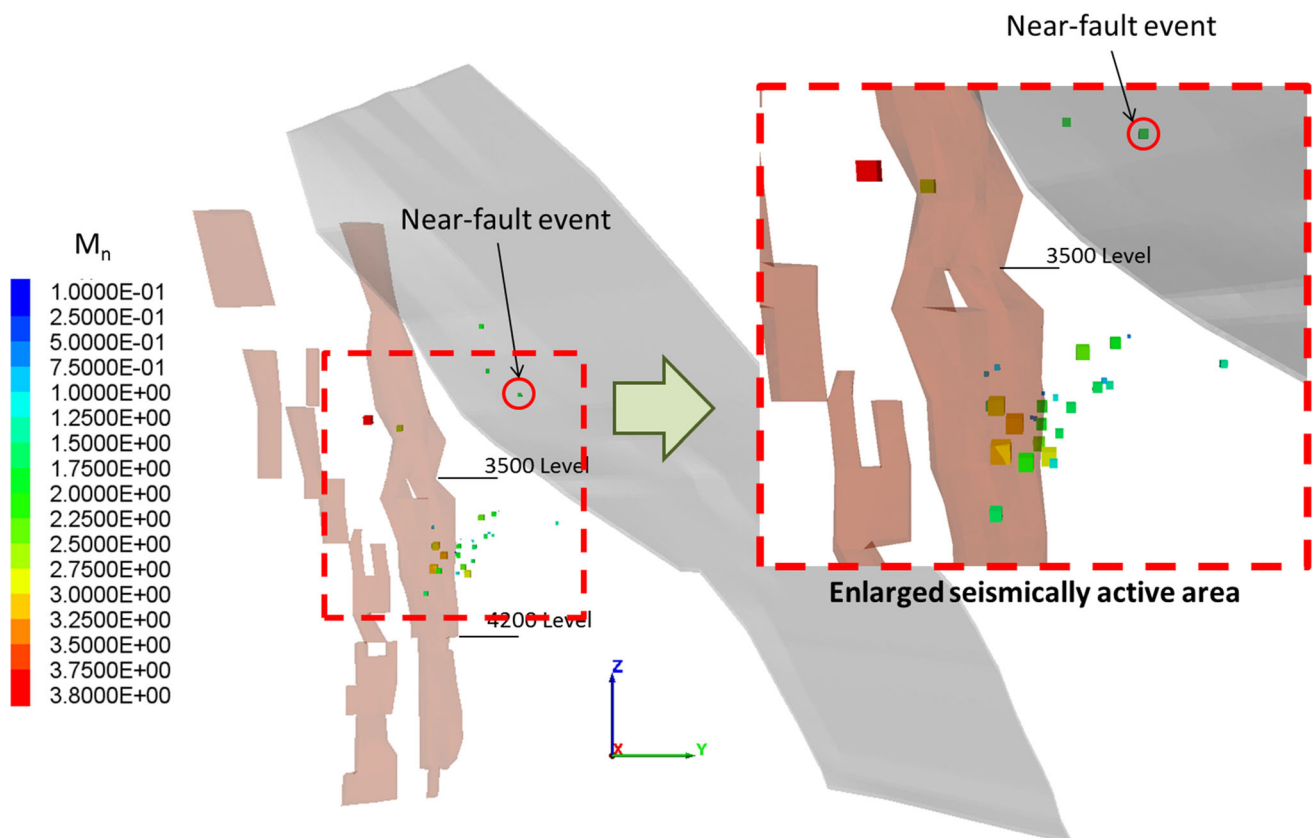


Fig. 12 Location of large seismic events that took place during the period from 2006 to 2014. The region surrounded by the broken line is seismically active

seismic events that take place within a distance of 15 m from the fault are regarded as near-fault events, considering the possible error. Importantly, the only one near-fault event shown in Fig. 12 took place immediately after the large seismic event with M_n of 3.8, indicating that it was an aftershock of the M_n 3.8 event, i.e. the near-fault event was possibly induced by transient stress caused by the M_n 3.8 event.

The fact that large seismic events barely take place near or within the fault verifies the results obtained from the numerical analysis. First, CFS_2 shown in Fig. 5b indicates that in extensive areas within the fault, the shear stress acting along the fault does not reach the maximum shear strength. Next, Fig. 8 reveals that the magnitude of increase in CFS_2 is not significant, considering negative values of CFS_2 at the pre-mining stage shown in Fig. 5b, and the influence of the mining activities on the stress state of the fault decreases as the mining stage proceeds. Subsequently, the static, elasto-plastic analysis demonstrates that the maximum shear displacement taking place during fault-slip is no more than 3 mm in static conditions, even immediately after the first mining stage in which stopes close to the fault are extracted. Lastly, the dynamic analysis conducted using the stress state after the first mining stage shows that the maximum slip rate during fault-slip is 30 cm/s at most, which is a considerably low value as a mine tremor and far below the threshold of peak particle

velocity that inflicts damage to the rockmass (Hedley 1992; Brinkmann 1987). All the results are in agreement with the fact that the fault is not seismically active.

7.2 Comparison with Microseismic Events

To further verify the postulation made in the previous sections, microseismic activities with moment magnitude down to -4 are investigated and analysed. Figure 13 shows locations of one hundred thousand microseismic events that took place during the period from 2004 to 2007. Due to the limitation of the software used, it was impossible to show all the seismic events (350,000) that took place from 2007 to 2014. As can be seen in the figure, microseismic events occur in the entire mine, and there are clusters of microseismic events. Obviously, locations of several clusters coincide with the orebodies modelled in the present study. Locations of the other cluster are associated with orebodies that are not the scope of the present study and/or locations of large seismic events that took place away from the active mining area (Sainoki et al. 2016). Figure 13 clearly shows that although microseismic events take place around the mine due to ore extraction, the rockmass near or within the fault is still seismically non-active. To verify the non-seismic activity, various seismic data analyses and comparison with the numerical analysis results are performed in what follows.

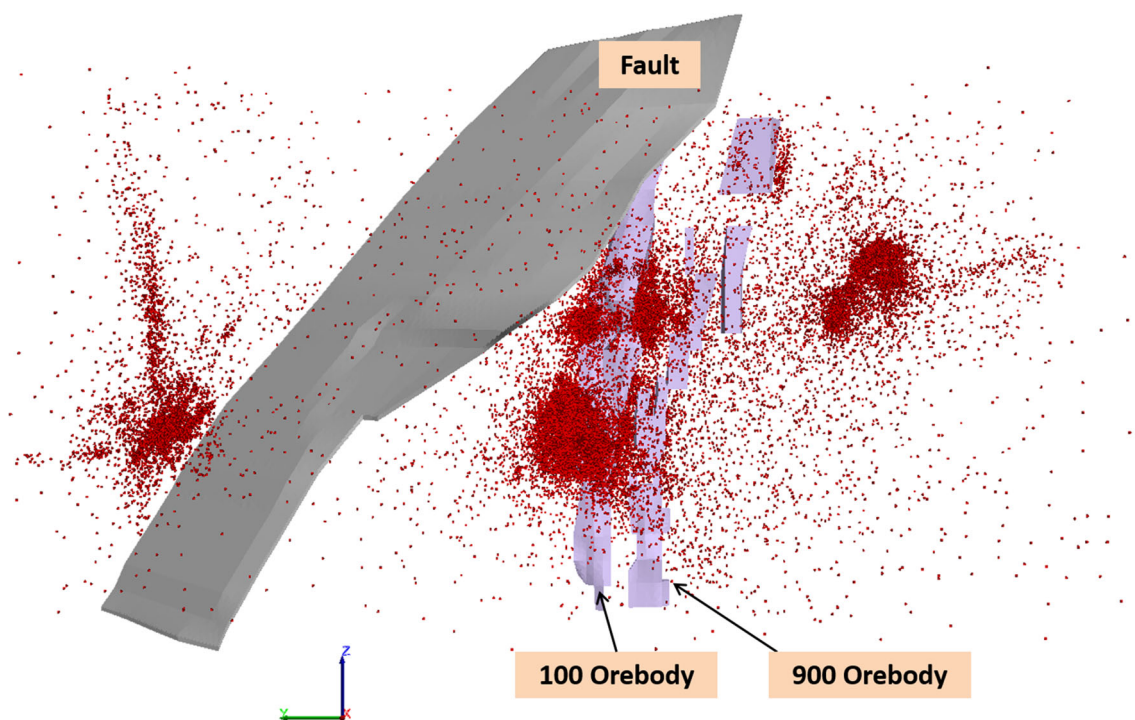


Fig. 13 Microseismic activities that took place from 2004 to 2007

Figure 14 shows plan views of intensity of microseismic activity as well as maximum shear strain increment for 3000 and 3500 Levels. In the figure, “intense” denotes that the number of microseismic events is greater than 10 in an area of $20\text{ m} \times 20\text{ m} \times 20\text{ m}$. As can be seen, seismic activity is quite dense near the orebodies, while seismic intensity is low near or within the fault. In contrast, the maximum shear strain increment is clearly large within the fault, indicating large deformations taking place in the fault due to elasto-plastic behaviour caused by ore extraction. Similar tendency is observed in Fig. 15 that shows the same data as in Fig. 14, but in cross sections in the y -direction. Figures 14 and 15 indicate that the shear deformations taking place in the fault do not release intense seismic energy, thus not contributing to the generation of severe seismic activity.

Figure 16 depicts the relation between the cumulative number of seismic events and time. According to Hudyma

and Beneteau (2012), when seismic source mechanism driven by geological structures is dominant, the cumulative number continuously increases, giving a constant event rate. On the contrary, when seismic events are caused by rock fracturing in response to production blasts, the cumulative number of events line shows a stepwise increase. As can be seen in Fig. 16, when considering near-fault events within 15 m, the increase in the cumulative number of seismic events is generally stepwise, implying that it is the result of production blasts, although at an early stage from 2004 to 2005, the cumulative number of events steadily increases. This may indicate that only in that short period, the fault was seismically active. When considering all seismic events, the number of seismic events start to exponentially increase from 2011, implying that seismic events caused by shearing of rockmass or other geological structures become dominant. Even then, the seismic activity in the fault is basically quiet.

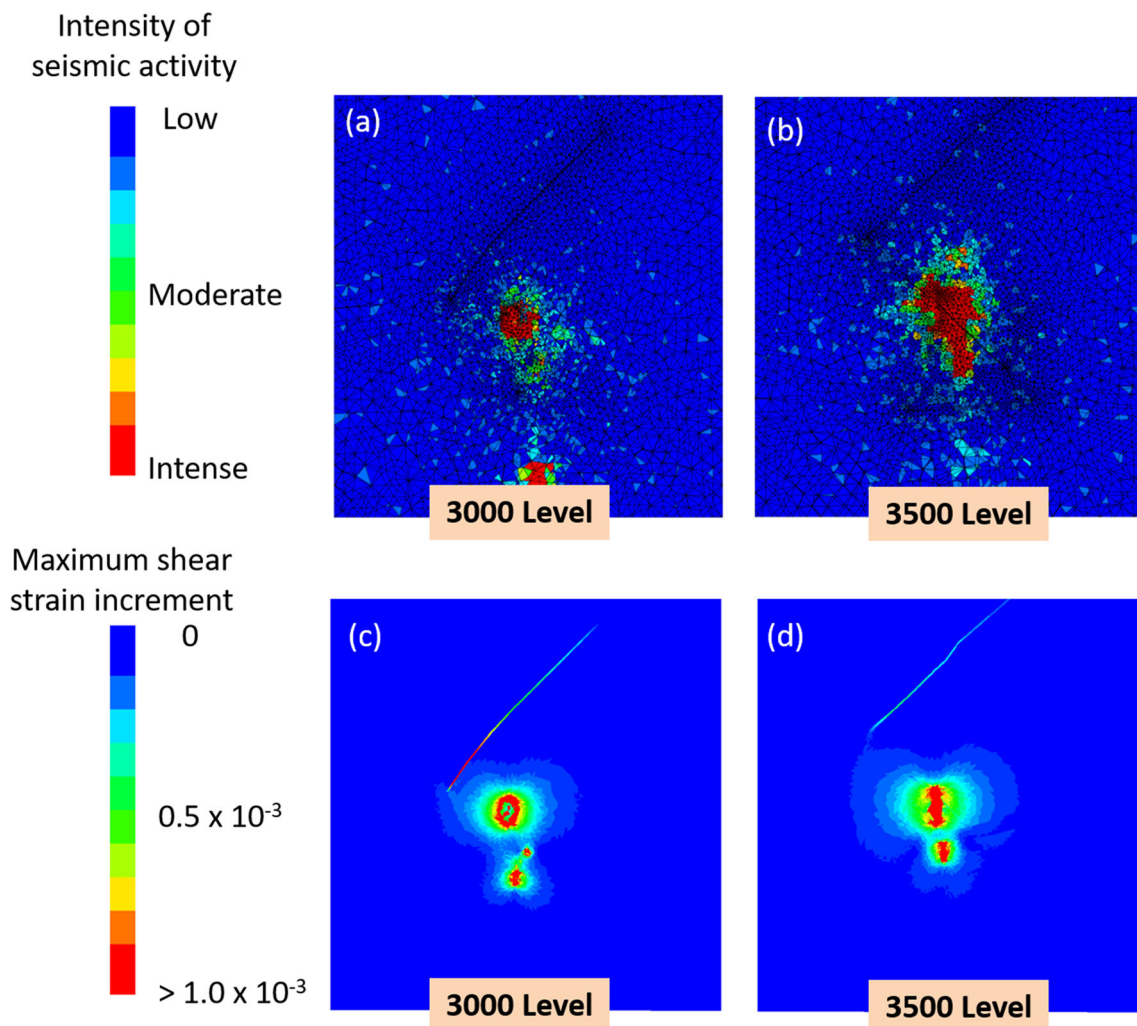


Fig. 14 Plan views showing the intensity of microseismic events and shear strain increment: **a** seismic intensity on 3000 Level, **b** seismic intensity on 3500 Level, **c** maximum shear strain increment on 3000 Level, and **d** maximum shear strain increment on 3500 Level

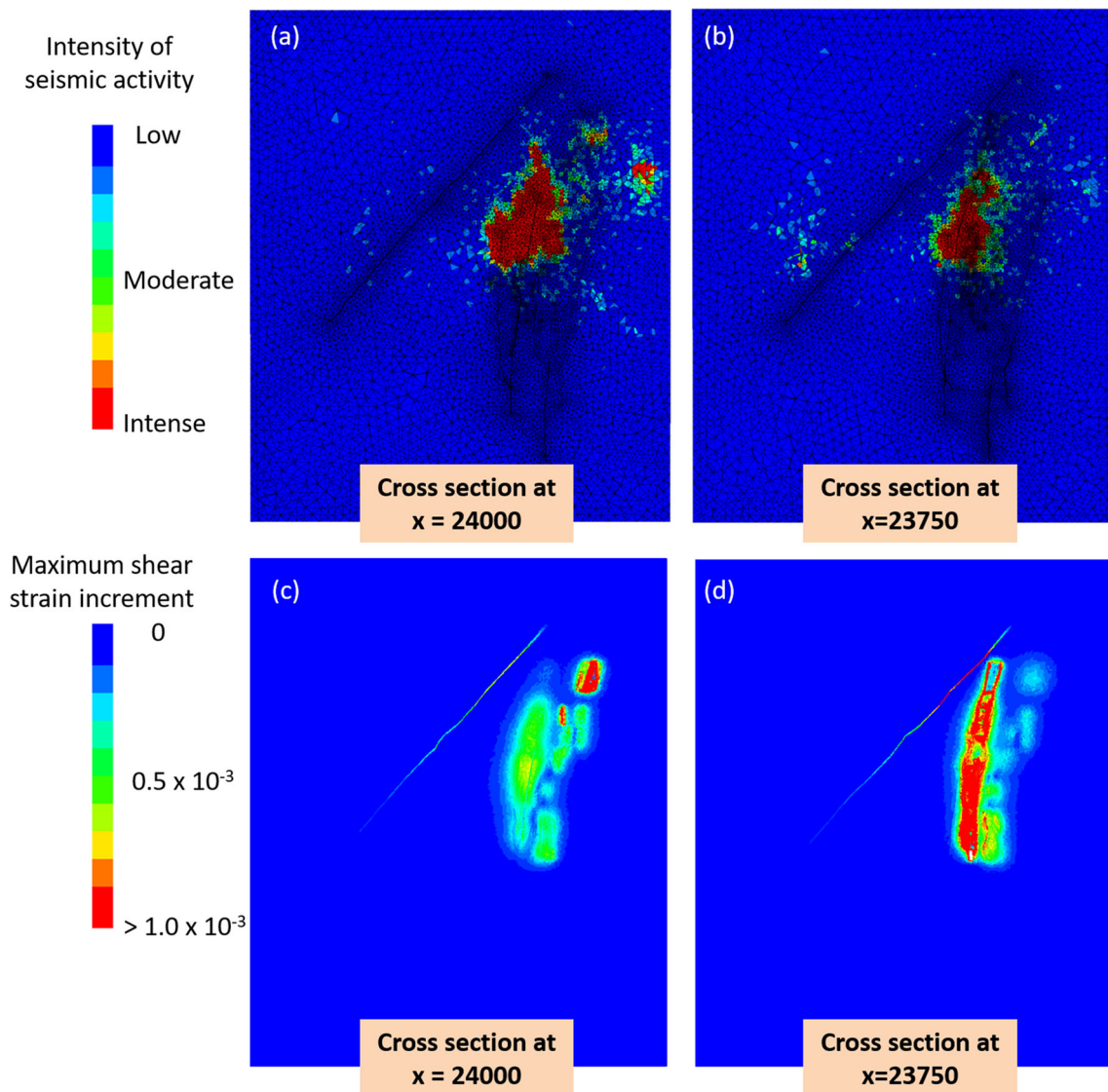


Fig. 15 Cross sections in the y -direction showing the intensity of microseismic events and shear strain increment: **a** seismic intensity on the cross section at $x = 24,000$, **b** seismic intensity on the cross

section at $x = 23,750$, **c** maximum shear strain increment on the cross section at $x = 24,000$, and **d** maximum shear strain increment on the cross section at $x = 23,750$

Figure 17 shows the results of time-between-events (TBE) analysis proposed by Hudyma and Beneteau (2012). The plots represent time between events for each event magnitude. As can be seen, the analysis was performed for near-fault events as well as the whole events. According to Hudyma and Beneteau (2012), high TBE rates denote seismic events driven by geological structures. As can be seen in Fig. 17, TBE rates of the fitted lines are in the range from 0.5 to 1.0. Obviously, the line for seismic events that took place within 15 m from the fault has the lowest TBE rate, implying that the events were caused by production blasts. Sainoki and Mitri (2016) conducted TBE analysis for a different underground hard rock mine in Canada, which showed that a TBE rate of 1.0 for seismic events

took place in a shear zone. These results further indicate that the fault in this mine is seismically non-active, although large shear deformation took place within the fault in response to ore extraction.

Table 4 lists the number of seismic events, cumulative seismic moment, and moment magnitude for near-fault events as well as the whole event. A comparison of the values with the numerical analysis result is also made. As mentioned above, 350,000 seismic events took place between 2004 and 2014. However, the number of seismic events that took place in the fault and within 15 and 30 m from the fault are merely 28, 87, and 201, respectively. In Table 4, the seismic moment computed from the numerical analysis is based on the deformation of the fault, meaning

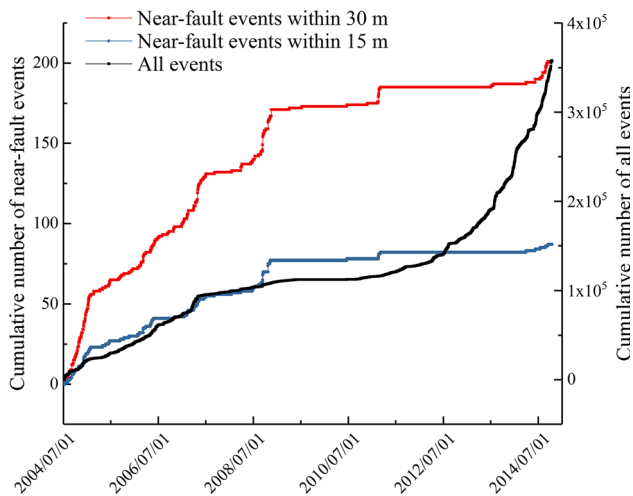


Fig. 16 Cumulative number of seismic events in the fault and all events

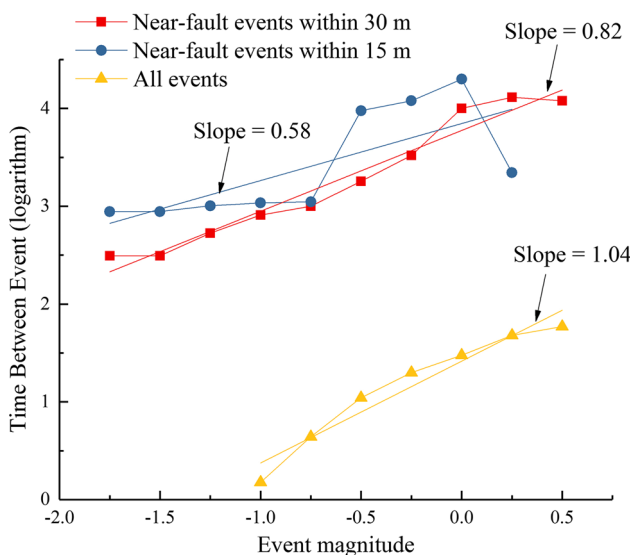


Fig. 17 Time-between-events (TBE) analysis for seismic events in the fault and in the whole region

that the value should be compared to cumulative seismic moment of seismic events in the fault. The comparison reveals that the computed seismic moment is 16 times higher than the measured cumulative seismic moment, thus strongly suggesting that the deformation of the fault did not release seismic energy, most likely because of the low slip

rate estimated with the dynamic analysis and the ductile behaviour of the fault material.

7.3 Discussion

The aforementioned results and discussion lead to the conclusion that a large seismic event associated with intense fault-slip is unlikely to occur along the fault. The slip caused by the mining activities is most likely aseismic and static. Furthermore, due to the low stress environment within the fault, the possibility of a large amount of seismic energy being released is considerably low. It should be noted, however, that it is not beyond the realm of possibility that a large seismic event occurs if severe strength heterogeneity is locally present within the fault. As demonstrated by Sainoki and Mitri (2016), the heterogeneity of shear stiffness within a shear zone can generate slip potential that is high enough to cause a large seismic event. Therefore, if such a condition had been present within the fault before the mining activities were started, a large seismic event may occur due to the induced stress concentration and the mining-induced stress re-distribution, i.e. the increase in CFS_2 . However, as no large seismic event took place within the fault in the past nine years in spite of the mining activities, the possibility that the noticeable heterogeneity of stiffness exists within the fault is presumably low. If such anomalies had been scattered within the fault, relatively large seismic events would have taken place during the past mining stages.

Regarding the shear failure examined with CFS_1 , the following conclusion can be drawn. Figure 5a indicates that the fault material had undergone shear failure in the plane of principal stresses at the pre-mining stress state, and Fig. 7 shows that the post-peak shear behaviour had taken place in the plane of principal stresses due to past mining sequences, due to the increase in CFS_1 . Notwithstanding these results, major seismic events did not occur within the fault. Furthermore, microseismic database analysis using 350,000 events that took place between 2004 and 2014 shows that only less than 100 seismic events did occur near or within the fault, and the events were caused by production blasts rather than active fault behaviour. It is thus reasonable to postulate that the post-peak shear behaviour does not contribute to the generation of major seismic events. The post-peak shear behaviour may

Table 4 Comparison of measured seismic parameters with numerical analysis

	Seismic events	Seismic moment	Moment magnitude
Events within the fault	28	1.0×10^{10}	0.64
Near-fault events within 15 m	87	2.1×10^{10}	0.85
Near-fault events within 30 m	201	1.0×10^{11}	1.31
Numerical analysis	N/A	1.6×10^{11}	1.46

produce minor seismic events with small magnitude, but such seismic events would not pose serious risks to underground openings and be characterized as steady fault activity, as shown by Naoi et al. (2015). From the results and discussion, it can be concluded that the post-peak shear behaviour of the fault material is aseismic and static shear movements with a low slip rate that do not generate intense seismic waves, even if sudden slip-weakening entailing a decrease in the friction angle takes place, because of the low stress environment in the fault and fractured rockmass.

Figure 18 summarizes the numerical and data analyses as a simplified flowchart. The data analysis starts with examining the occurrence of seismic events in a fault zone. Provided that there are near-fault events, TBE and time history analyses can be performed to determine whether or not the fault is seismically active. As for numerical analysis, CFS and shear strain increment are investigated. Then, if $CFS > 0$ and there are certain shear strain increments in the fault, dynamic analysis should be performed to quantitatively evaluate the dynamic behaviour of the fault in terms of slip rate. A low slip rate less than 0.3 m/s is indicative of aseismic behaviour of the fault. However, when there is strong heterogeneity in terms of shear

stiffness within the fault, a large seismic event could occur due to stress concentration that evolves in the stiff inclusion within the fault. In this way, fault behaviour characterization and risk analysis for a large seismic event can be performed.

As the shear movements within and along the target fault do not contribute to the generation of major seismic events, the exclusive use of seismic moment computed from the shear movement leads to unnecessary precautions, as suggested by Sjöberg et al. (2012). Instead of seismic moment, stress re-distribution near the stopes induced by the aseismic slip movements should be considered and examined when dynamic slip rates are predominantly aseismic and do not cause severe seismicity. This is because there is a possibility that the induced slip movements have an influence on the stress state in the vicinity of stopes and may trigger seismic events as reported by White and Whyatt (1999). The present study suggests that the use of static and dynamic analyses in conjunction with seismic database gives more appropriate suggestions that consider aseismic fault-slip. However, it is to be noted that although the present study implies that fault-slip is aseismic or does not lead to a large seismic event when the slip rate of a

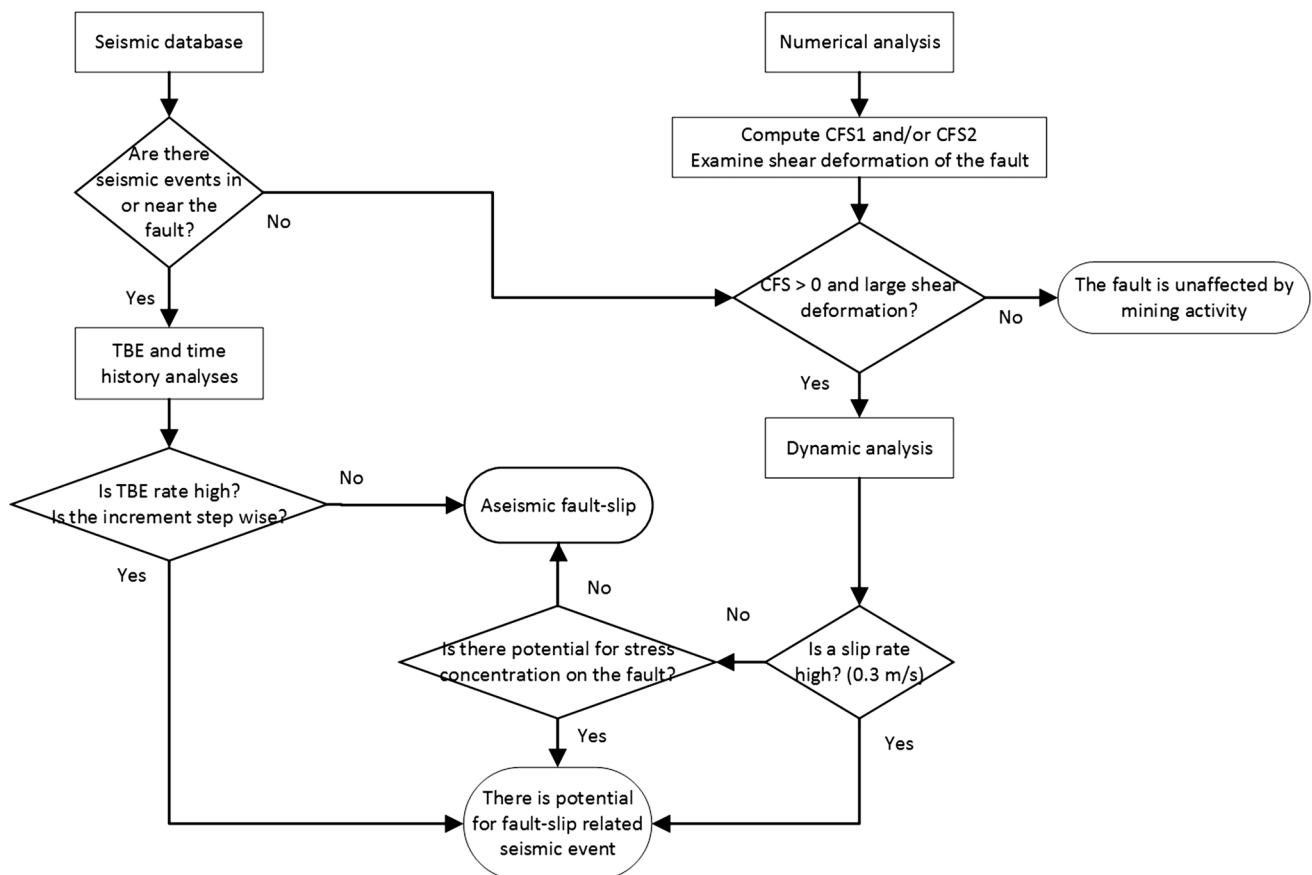


Fig. 18 Flowchart to assess the degree of seismic activity in a fault and to distinguish aseismic fault-slip with numerical analysis and seismic database analysis

fault during fault-slip is estimated to be less than 0.3 m/s, more evidence from seismic field studies is required to ascertain the level of slip beyond which the fault-slip may be considered seismic. The numerical analyses and discussion conducted in this study contribute to developing a methodology for distinguishing aseismic from seismic fault-slip, consequently helping mining engineers propose more appropriate support designs for fault-slip.

8 Conclusions

In the present study, the stress state and behaviour of the 900 Orebody Cross fault in Copper Cliff Mine are examined through back analysis for developing a methodology to distinguish aseismic from seismic fault-slip. Aseismic fault-slip is characterized as the static shear movement of a fault with a low slip rate that does not generate intense seismic waves, while seismic fault-slip could generate intense seismic waves with high slip rates that might cause severe damage to underground openings. A 3D numerical model encompassing major geological structures in the region of interest is first constructed. Subsequently, three types of analyses are performed, namely elastic and elasto-plastic analyses in static conditions and elasto-plastic analysis in dynamic conditions. The results obtained from the elastic and elasto-plastic analyses in static conditions indicate the possibility of shear failure taking place along the fault or in the plane of principal stresses. Notwithstanding these results, in situ seismic-monitoring system detected no major seismic events within the fault, with the exception of one event that took place in the footwall rock immediately after a large seismic event with M_n of 3.8. This suggests that the shear movements taking place along and within the fault are aseismic and static. Furthermore, microseismic database analysis using 350,000 events that took place between 2004 and 2014 indicates that the fault is not seismically active. The elasto-plastic analysis in dynamic conditions confirms that the slip rate of the fault is at most 0.30 m/s, even when the fault-slip is driven by an instantaneous stress drop due to the transition from static to kinetic friction. These results indicate that relying on seismic moment alone for assessing fault-slip potential is not appropriate. The present study sheds light on the importance of distinguishing aseismic from seismic fault-slip for optimizing underground support systems. It is believed that this work has contributed to better understanding of fault behaviour and its consequence during the ore extraction process.

Acknowledgements This work is financially supported by a grant by the Natural Science and Engineering Research Council of Canada (NSERC) in partnership with Vale Ltd—Sudbury Operations,

Canada, under the Collaborative Research and Development Program. The authors are grateful for their support.

References

- ABAQUS (2003) ABAQUS online documentation: Ver 6.4-1.: Dassault Systemes, France
- Alber M, Fritschen R (2011) Rock mechanical analysis of a $M1 = 4.0$ seismic event induced by mining in the Saar District, Germany. *Geophys J Int* 186:359–372
- Alber M, Fritschen R, Bischoff M, Meier T (2009) Rock mechanical investigations of seismic events in a deep longwall coal mine. *Int J Rock Mech Min Sci* 46:408–420
- Altindag R, Guney A (2010) Predicting the relationships between brittleness and mechanical properties (UCS, TS and SH) of rocks. *Sci Res Essay* 5:2107–2118
- Bandis S, Lumsden AC, Barton NR (1983) Fundamentals of rock joint deformation. *Int J Rock Mech Min Sci Geomech* 20:249–268
- Barton N (1973) Review of a new shear-strength criterion for rock joints. *Eng Geol* 7:287–332
- Bewick RP, Valley B, Runnals S, Whitney J, Krynicki Y (2009) Global approach to managing deep mining hazard. In: The 3rd CANUS rock mechanics symposium, Toronto
- Bieniawski ZT (ed) (1976) Rock mass classification in rock engineering. In: Exploration for rock engineering. Balkema, Cape Town
- Blake W, Hedley DGF (2003) Rockbursts case studies from North America hard-rock mines. Society for Mining, Metallurgy, and Exploration, Littleton
- Brinkmann JR (1987) Separating shock wave and gas expansion breakage mechanism. In: 2nd international symposium on rock fragmentation by blasting
- Cai M (2010) Practical estimates of tensile strength and Hoek–Brown strength parameter m_i of brittle rocks. *Rock Mech Rock Eng* 43:167–184
- Cappa F, Rutqvist J (2011) Modeling of coupled deformation and permeability evolution during fault reactivation induced by deep underground injection of CO₂. *Int J Greenhouse Gas Control* 5:336–346
- Cappa F, Rutqvist J (2012) Seismic rupture and ground accelerations induced by CO₂ injection in the shallow crust. *Geophys J Int* 190:1784–1789
- Dieterich JH (1979) Modeling of rock friction I. Experimental results and constitutive equations. *J Geophys Res* 84:2161–2168
- Dieterich JH, Kilgore B (1996) Implications of fault constitutive properties for earthquake prediction. In: Proceedings of the National academy of science, U.S.A., pp 3787–3794
- ESG (2011) WaveVis. ESG solutions, Kingston
- Fischer-Cripps AC, Mustafaev I (2000) Introduction to contact mechanics. Springer, New York
- Gibowicz SJ, Kijko A (1994) An introduction to mining seismology. Academic Press, London
- Hedley DGF (1992) Rockburst handbook for ontario hard rock mines. Ontario Mining Association, North York
- Hergert G (1987) Stress assumptions for underground excavations in the Canadian Shield. *Int J Rock Mech Min Sci Geomech Abstr* 24:95–97
- Hoek E (2007) Practical rock engineering. Rocscience. <https://www.rocscience.com/documents/hoek/corner/Practical-Rock-Engineering-Full-Text.pdf>
- Hoek E, Brown ET (1997) Practical estimates of rock mass strength. *Int J Rock Mech Min Sci* 34:1165–1186

- Hoek E, Carranza-Torres C, Corkum B (2002) Hoek–Brown failure criterion—2002 edition. In: NARMS-TAC conference, 2002 Toronto, pp 267–273
- Hofmann GF, Scheepers LJ (2011) Simulating fault slip areas of mining induced seismic tremors using static boundary element numerical modelling. *Min Technol* 120:53–64
- Hudyma M, Beneteau DL (2012) Time—a key seismic source parameter. In: Hawkes C (ed) 21st Canadian rock mechanics symposium ROCKENG12—rock engineering for natural resources, 2012. The Canadian Rock Mechanics Association, pp 311–318
- Ida Y (1972) Cohesive force across the tip of a longitudinal-shear crack and Griffith's specific surface energy. *J Geophys Res* 77:3769–3778
- ITASCA (2009) FLAC3D—fast Lagrangian analysis of continua. 4.0 edn. Itasca Consulting Group Inc., USA
- ITASCA Consulting Group I (2013). Kubrix Ver. 12. Itasca, Minneapolis
- Kanamori H (2001) Energy budget of earthquakes and seismic efficiency. *Int Geophys* 76:293–305
- Lizurek G, Rudziński Ł, Plesiewicz B (2015) Mining induced seismic event on inactive fault. *Acta Geophys* 63:176–200
- Lockner DA, Byerlee JD, Kuksenko V, Ponomarev A, Sidrin A (1991) Quasi-static fault growth and shear fracture energy in granite. *Nature* 350:39–42
- Lysmer J, Kuhlemeyer RL (1969) Finite dynamic model for infinite media. *J Eng Mech* 95:859–877
- Marinos P, Hoek E (2001) Estimating the geotechnical properties of heterogeneous rock masses such as Flysch. *Bull Eng Geol Environ* 60:85–92
- McGarr A (1991) Observations constraining near-source ground motion estimated from locally recorded seismograms. *J Geophys Res* 96:16495–16508
- McGarr A (1994) Some comparisons between mining-induced and laboratory earthquakes. *PAGEOPH* 142:467–489
- McGarr A (2002) Control of strong ground motion of mining-induced earthquakes by the strength of the seismogenic rock mass. *J S Afr Inst Min Metall* 102:225–229
- McNeel R & Associates (2015) Rhinoceros 3D, Version 5.0. Robert McNeel & Associates, Seattle, WA
- Naoi M, Nakatani M, Otsuka K, Yabe Y, Kgarume T, Murakami O, Masakale T, Ribeiro L, Ward A, Moriya H, Kawataka H, Durrheim R, Ogasawara H (2015) Steady activity of microfractures on geological faults loaded by mining stress. *Tectonophysics* 649:100–114
- Ohnaka M, Akatsu M, Mochizuki H, Oedra A, Tagashira F, Yamamoto Y (1997) A constitutive law for the shear failure of rock under lithospheric conditions. *Tectonophysics* 277:1–27
- Okubo PG, Dieterich JH (1984) Effects of physical fault properties on frictional instabilities produced on simulated faults. *J Geophys Res* 89:5817–5827
- Ortlepp WD (2000) Observation of mining-induced faults in an intact rock mass at depth. *Int J Rock Mech Min Sci* 37:423–426
- Ortlepp WD, Stacey TR (1994) Rockburst mechanisms in tunnels and shafts. *Tunn Undergr Space Technol* 9:59–65
- Potvin Y, Jarufe J, Wesseloo J (2010) Interpretation of seismic data and numerical modelling of fault reactivation at El Teniente, Reservas Norte sector. *Min Technol* 119:175–181
- Ruina A (1983) Slip instability and state variable friction laws. *J Geophys Res* 88:10359–10370
- Rutqvist J, Cappa F, Mazzoldi A, Rinaldi A (2013) Geomechanical modeling of fault response and the potential for notable seismic events during underground CO₂ injection. *Energy Procedia* 37:4774–4784
- Ryder JA (1988) Excess shear stress in the assessment of geologically hazardous situations. *J S Afr Inst Min Metall* 88:27–39
- Sainoki A, Mitri HS (2014a) Dynamic modelling of fault slip with Barton's shear strength model. *Int J Rock Mech Min Sci* 67:155–163
- Sainoki A, Mitri HS (2014b) Evaluation of fault-slip potential due to shearing of fault asperities. *Can Geotech J* 52:1417–1425
- Sainoki A, Mitri HS (2015) Effect of slip-weakening distance on selected seismic source parameters of mining-induced fault-slip. *Int J Rock Mech Min Sci* 73:115–122
- Sainoki A, Mitri HS (2016) Back analysis of fault-slip in burst prone environment. *J Appl Geophys* 134:159–171
- Sainoki A, Mitri HS, Yao M, Chinnasane D (2016) Discontinuum modelling approach for stress analysis at a seismic source: case study. *Rock Mech Rock Eng* 49:4749–4765
- Shnorhokian S, Mitri HS, Thibodeau D (2014) A methodology for calibrating numerical models with a heterogeneous rockmass. *Int J Rock Mech Min Sci* 70:353–367
- Sjöberg J, Perman F, Quinteiro C, Malmgren L, Dahner-Lindkvist J, Boskovic M (2012) Numerical analysis of alternative mining sequences to minimise potential for fault slip rockbursting. *Min Technol* 121:226–235
- Snelling PE, Godin L, McKinnon SD (2013) The role of geologic structure and stress in triggering remote seismicity in Creighton Mine, Sudbury, Canada. *Int J Rock Mech Min Sci* 58:166–179
- Trifu CI, Urbancic TI (1996) Fracture coalescence as a mechanism for earthquake: observations based on mining induced microseismicity. *Tectonophysics* 261:193–207
- Urbancic TI, Trifu C-I (1998) Shear zone stress release heterogeneity associated with two mining-induced events of M 1.7 and 2.2. *Tectonophysics* 289:75–89
- Urpi L, Rinaldi A, Rutqvist J, Cappa F, Spiers C (2016) Dynamic simulation of CO₂-injection-induced fault rupture with slip-rate dependent friction coefficient. *Geomech Energy Environ* 7:47–65
- Van Gool B (2007) Effects of blasting on the stability of paste fill stopes at Cannington Mine. PhD, James Cook University
- White BG, Whyatt JK (1999) Role of fault slip on mechanisms of rock burst damage, Lucky Friday Mine, Idaho, USA. In: 2nd southern african rock engineering symposium, Implementing Rock Engineering Knowledge. Johannesburg, S. Africa
- Wyllie DC (2003) Foundations on rock: engineering practice, 2nd edn. CRC Press, Boca Raton
- Yabe Y, Nakatani M, Naoi M, Philipp J, Janssen C, Watanabe T, Katsura T, Kawataka H, Georg D, Ogasawara H (2015) Nucleation process of an M2 earthquake in a deep gold mine in South Africa inferred from on-fault foreshock activity. *J Geophys Res Solid Earth* 120:5574–5594
- Yuan F, Prakash V (2008) Use of a modified torsional Kolsky bar to study frictional slip resistance in rock-analog materials at coseismic slip rates. *Int J Solids Struct* 45:4247–4263
- Zhang P, Yang T, Yu Q, Xu T, Zhu W, Liu H, Zhou J, Zhao Y (2015) Microseismicity induced by fault activation during the fracture process of a crown pillar. *Rock Mech Rock Eng* 48:1673–1682
- Ziegler M, Reiter K, Heidbach O, Zang A, Kwiatek G, Stromeyer D, Dahm T, Dresen G, Hofmann G (2015) Mining-induced stress transfer and its relation to a Mw 1.9 seismic event in an ultra-deep South African gold mine. *Pure Appl Geophys* 172:2557–2570